



111
212
THS



This is to certify that the

thesis entitled

An Experimental Study into
The Nonlinear Behavior of
A Parabolic Arch Bridge

presented by

Bruce Frazier Henley

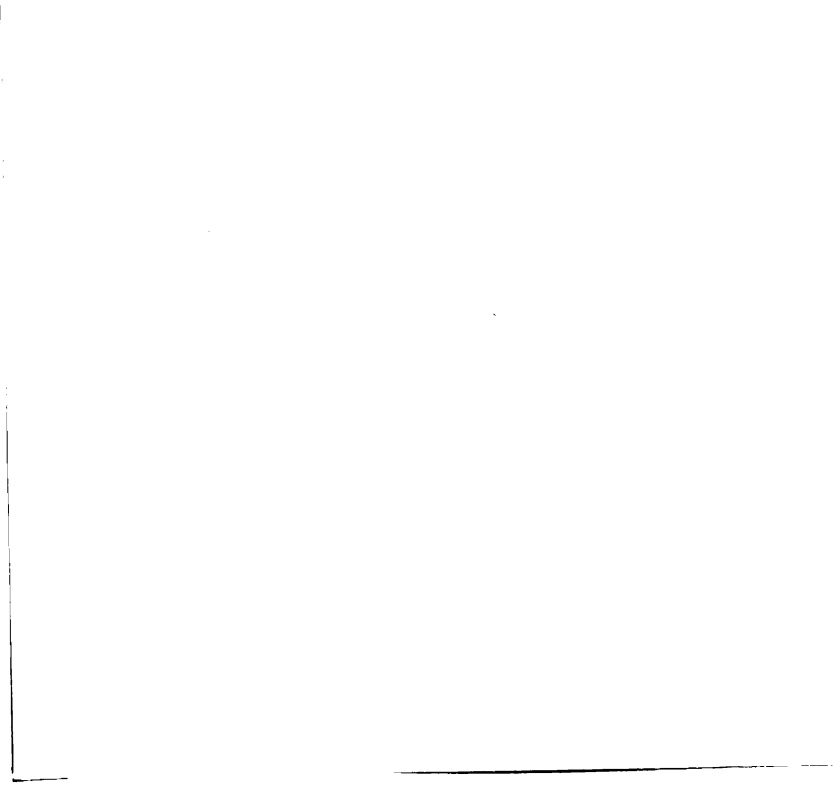
has been accepted towards fulfillment
of the requirements for
Department of
Master of degree in Civil Engineering
Science

Major professor

Date November 16, 1977

~~SECRET~~

#BX B/82



AN EXPERIMENTAL STUDY INTO THE NONLINEAR
BEHAVIOR OF A PARABOLIC ARCH BRIDGE

By
Bruce Frazier Henley

A THESIS

Submitted to
Michigan State University
in partial fulfillment of the requirements
for the degree of

MASTER OF SCIENCE

Department of Civil Engineering

1977

ABSTRACT

AN EXPERIMENTAL STUDY INTO THE NONLINEAR BEHAVIOR OF A PARABOLIC ARCH BRIDGE

By

Bruce Frazier Henley

An experimental study of the nonlinear behavior of a parabolic arch bridge model, up to the point of buckling, is reported. The bridge model is 96 inches long, and has a rise of $16\frac{1}{2}$ inches, and the ribs are 4 inches center to center and connected by lateral bracing beams at every 6 inches on the horizontal projection.

Vertical and lateral loads were applied in various combinations to simulate actual load conditions. By applying the load increments in a monotonic manner, the behavior of the bridge could be observed and measured.

It was found that the symmetric and antisymmetric buckling modes are in close proximity of each other, but that the symmetric mode appears to be the failure mode. Several techniques were used to deduce the buckling load, and the

load-displacement asymptote and Southwell plot methods worked reasonably well for both modes.

The decrease of lateral stiffness due to vertical loads was also studied. However, the buckling load extrapolated from these results appears to be too low.

ACKNOWLEDGMENTS

The work reported herein has been supported by the Division of Engineering Research, and also by the Department of Civil Engineering.

This work constitutes the author's thesis, which has been written under the direction of Dr. Robert K. Wen, to whom deepest gratitude is extended for his guidance and instruction.

The author wishes to express his appreciation to his fellow graduate students, Tom Heck and Jose Lange for their assistance in the collection of the data. Special gratitude is extended to the Machine Shop of the College of Engineering for their assistance in fabricating the experimental apparatus.

TABLE OF CONTENTS

Chapter	Page
I INTRODUCTION.....	1
1.1 Object and Scope.....	1
1.2 Notation.....	3
II DESIGN AND CONSTRUCTION OF MODEL.....	5
2.1 General.....	5
2.2 Demensional Analysis.....	5
2.3 Properties of the Model.....	6
2.4 Computer Analysis.....	9
2.5 Test Apparatus and Construction.....	11
2.5.1 Arch Ribs and Bracing.....	11
2.5.2 End Supports.....	14
2.5.3 Panel Joints.....	14
2.5.4 Loads.....	14
2.5.5 Measurement Equipment.....	16
III TEST PROCEDURES.....	18
3.1 Vertical Load-Only Tests.....	18
3.2 Combined Lateral and Vertical Load Tests....	19
IV RESULTS AND DISCUSSION.....	21
4.1 General.....	21
4.2 Behavior Under Vertical Loads-Only.....	21
4.2.1 Overall Behavior.....	21
4.2.2 Crown Behavior.....	22
4.2.3 Quarter Point Behavior.....	32
4.3 Behavior Under Combined Lateral and Vertical loads.....	32
4.3.1 Overall Behavior.....	32
4.3.2 Crown Behavior.....	33
4.4 Buckling Load.....	34
4.4.1 Vertical Load-Only.....	34
4.4.2 Combined Load Testing.....	35
4.5 Discussion.....	40
4.5.1 Differences Among Test Results.....	40
4.5.2 Comparisons with the Results of Others.....	42

Table of Contents (Continued)

Chapter	Page
V CONCLUSION.....	46
LIST OF REFERENCES.....	49

LIST OF TABLES

Table		Page
2-1	Dimensional Analysis Parameters and Values.....	7
2-2	Properties of the Ribs and Bracing.....	8
4-1	Tabulation of Experimental Buckling Loads.....	41

LIST OF FIGURES

Figure	Page
2-1 Arch Bridge Test Model.....	10
2-2 Front View of Model.....	12
2-3 End View of Model.....	12
2-4 Bracing.....	13
2-5 Hinges.....	13
2-6 Panel Joint.....	15
4-1 Displaced Shape of One Rib Under Typical Vertical Load-Only Test.....	23
4-2 Load-Displacement Curve for the Crown Under Vertical Loads-Only.....	25
4-3 Load-Displacement Plot for the Antisymmetric Component of Δ_2	26
4-4 Load-Displacement Plot for the Symmetric Component of Δ_2	27
4-5 Displaced Shape of One Rib Under Typical Combined Load Tests.....	28
4-6 Load-Displacement Plots for the Crown Under Combined Load Tests ($q=0.0, 1.0, 1.8, 2.7, 3.7$)..	29
4-7 Load-Displacement Plots for the Crown Under Combined Load Tests ($q=0.7, 1.3, 2.2, 3.0$).....	30
4-8 Load-Displacement Plots for the Crown Under Combined Load Tests ($q=0.8, 1.5, 2.5, 3.3$).....	31
4-9 Lateral Stiffness versus Vertical Load.....	36

List of Figures (Continued)

Figure		Page
4-10	Southwell Plot for the Crown.....	37
4-11	Southwell Plot for the Antisymmetric Component of Δ_2	38
4-12	Southwell Plot for the Symmetric Component of Δ_2	39

I. INTRODUCTION

1.1 Object and Scope

Arches are one of the oldest type of structures. In the days of the Roman Empire, arch bridges were built with masonry materials. Due to a lack of analytical knowledge, the design and construction of those structures were essentially based on experience. Because of their bulkiness, elastic stability usually was not a problem. The strength of masonry, however, limited the size and span length of those old structures.

The introduction of steel and the development of structural mechanics in the 18th Century greatly extended the capability of structural engineers. Arch bridges of increasingly long spans were built. For example, the Kill Van Kull bridge in New York has a 1,675 foot span.

The more recent advent of the computer has further enabled the engineer to make increasingly more precise calculations. There is a tendency to use lighter and more slender construction. As the span lengths have increased, their relative widths have decreased. This produces a long slender arch bridge, which renders itself more susceptible to geometric instabilities. A study of the behavior of long slender arch bridges, up to or near the buckling load, could show the significance of the bracing upon the overall

stability of the arch bridge. To date, the buckling load of a single parabolic arch rib has been studied both analytically and experimentally by a number of investigators (see, for example, References 5 and 7). Available studies of the entire arch bridge, a structural system that consists of two ribs with one of several commonly used bracing patterns, have been rather limited in their scope and numbers. It is this lack of information concerning the nonlinear behavior, to the point of buckling, that has stimulated this investigation, the ultimate goal being to aid in the design of the bracing system to provide a more stable bridge.

The present study is limited to investigating the nonlinear behavior of a through type parabolic arch bridge with Vierendeel bracing. The investigation is to be carried out by experimental study of a long slender arch bridge. This is accomplished in essentially two phases: First, the design and construction of a model based on prototype designs; secondly, the execution and analysis of a series of loading tests. With a knowledge of the displacements at the crown and quarter points, the buckling load can be determined without damaging the model.

Two loading conditions were employed in this study. First, a vertical load only test sequence, simulating live load plus dead load, was performed to obtain a vertical load-lateral displacement relationship, hereinafter to be called the vertical load-displacement relation. Secondly, a combined vertical and lateral load, simulating wind load, test series was performed to provide a lateral load-lateral

displacement relation, similarly this will be termed the lateral load-displacement relation, with the vertical load as a parameter. Reduction of the data obtained provided reasonable agreement as to the buckling load when estimated by the asymptote estimation of the load-displacement plots and by the Southwell plots.

The decrease of lateral stiffness due to vertical loads was also studied. However, the buckling load extrapolation from these results appears to be too low.

In the following chapters, Chapter II contains a description of the dimensional analysis, design, computer analysis, and construction of the laboratory model. The test procedures are outlined in Chapter III. The results are presented in Chapter IV along with a discussion of their meaning. A summary of this report is then contained in Chapter V.

1.2 Notation

The symbols used herein are listed below with their definitions:

A	Cross sectional area (in. ²)
C	Torsional constant (in. ⁴)
E	Young's modulus (lbs./in. ²)
H	Rise of the crown above the hinges (in.)
h	Width of bridge (c. to c. of arch ribs)(in.)
I _{xx}	Major axis moment of inertia (in. ⁴)
I _{yy}	Minor axis moment of inertia (in. ⁴)
J	Polar moment of inertia (in. ⁴)
K _h	Lateral stiffness of bridge (lbs./in.)
L	Span length (in.)

q	Vertical load (lbs./inch of bridge)
S	Panel width (in.)
w	Lateral load (lbs./inch of bridge)
Δ	Lateral displacement (in.)
$\Delta_1, \Delta_2, \Delta_3, \Delta'_2$	Dial gages readings along bridge
Δ_2^*	Asymmetric component of recorded Δ_2
Δ_2^{**}	Symmetric component of recorded Δ_2

Terms which appear with a bar ($\bar{\quad}$) over them represent quantities associated with the bracing, and unbarred terms refer to quantities associated with the arch ribs.

II. DESIGN AND CONSTRUCTION OF MODEL

2.1 General

Before a realistic model of an arch bridge can be constructed, it is important to first obtain the values of certain parameters of existing "prototype" bridges. Then with the aid of dimensional analysis, the ranges of values of the properties of the model can be formulated. After the shapes and other properties of the model have been established, a numerical solution can be obtained to get a feel for the forces and displacements produced by the applied loads. After the numerical solution showed what appeared to be acceptable behavior, the physical model was then constructed. The following three sections will deal more specifically with the above mentioned topics, along with the test set-up.

2.2 Dimensional Analysis

The fundamental objective of dimensional analysis is to reduce the number of independent variables, and establish a set of dimensionless variables that will ensure proper similitude between the physical systems (1). The dimensionless parameters chosen for this investigation are listed in Column (1) of Table 2-1.

The next step is to compute the "practical" range of values that would be used to create a model. This was

accomplished by computing the values of the dimensionless parameters corresponding to four real arch bridges: the Cold Spring Canyon bridge near Santa Barbara, California, the Ohio State Route 8 bridge near Cleveland, Ohio, the South Street bridge over I-84 near Middlebury, Connecticut, and the Colorado River bridge on Utah State Route 95. The ranges of such values for the above mentioned bridges are listed in column (2) of Table 2-1.

2.3 Properties of the Model

The dimensionless parameters and the "practical" ranges of values presented above would allow the creation of an infinite variety of model arch bridges. But if one or more of the independent variables can be solved for by fixing the value of say just one independent variable, the number of correct solutions for the remaining unsolved variables will be greatly reduced. Since the width of a testing frame in the Structures Laboratory and the length of a sheet of aluminum are both 96.0 inches, this was chosen for the length (L) of the bridge. Then by using Columns (1) and (2) in Table 2-1, direct substitution of L will yield values for the rise (H), width (h), bracing spacing (S), and the areas (A) and (\bar{A}). The remaining values are dependent upon the choice of the cross sections of the rib and bracing. This turns out to be an iterative process to obtain the most acceptable solution. Presented in Table 2-2 is the final choice for the sectional properties for both the ribs and the bracing. The corresponding values of the dimensionless parameters are listed in Column (3) of Table 2-1. It can be seen that not

TABLE 2-1 Dimensional Analysis Parameters and Values

Dimensionless Parameters	Desired Range	Values of Model		Tokarz's Values	
ν	0.30	0.32	X	0.32	X
H/L	0.13 → 0.17	0.17	X	0.2	
S/L	0.05 → 0.15	0.063	X	0.067	X
h/L	0.037 → 0.13	0.042	X	0.14	
\bar{I}_{xx}/I_{xx}	0.0095 → 0.035	0.026	X	0.032	X
\bar{I}_{yy}/I_{yy}	0.0015 → 0.014	0.13		0.00052	
\bar{A}/A	0.10 → 0.25	0.24	X	0.067	
$\bar{C}/C = \bar{J}/J$	(0.35 → 3.5)x10 ⁻⁴	0.087		0.0011	X
I_{yy}/I_{xx}	0.10 → 0.65	0.12	X	0.016	
J/I_{yy}	2.5 → 10.5	9.39	X	1.02	
I_{xx}/A^2	1.7 → 5.1	0.74	X	0.74	X
L/\sqrt{A}	197.1 → 429.5	217.8	X	111.8	
GC/EI_{yy}	1.79 → 7.50	3.56	X	0.75	
$w/E\sqrt{A}$	(1.4 → 2.6)x10 ⁻⁷			N.A.	
$q/E\sqrt{A}$	(1.3 → 2.2)x10 ⁻⁶			?	

* ---(x) indicates that the value is within the range of existing bridges.

TABLE 2-2 Properties of the Ribs and Bracing

Span Length,	L	=	96.0 in.
Rise,	H	=	16.25 in.
Bracing Spacing,	S	=	6.0 in.
Width,	h	=	4.0 in.
(Cross Section) rib,		=	0.75 deep x 0.26 in. wide
Area,	A	=	0.1943 in ²
Torsional Constant,	C	=	3.40 x 10 ⁻³ in ⁴
Moments of Inertia,	I _{xx}	=	9.10 x 10 ⁻³ in ⁴
	I _{yy}	=	1.08 x 10 ⁻³ in
(Cross Section) brace,		=	0.25 deep x 0.188 in. wide
Area,	A	=	0.0469 in ²
Torsional Constant,	\bar{C}	=	2.97 x 10 ⁻⁴ in ⁴
Moments of Inertia,	\bar{I}_{xx}	=	2.44 x 10 ⁻⁴ in ⁴
	\bar{I}_{yy}	=	1.37 x 10 ⁻⁴ in ⁴

all of the dimensionless values fall in the desired ranges. This is due to the necessity of having to use solid cross-sections for both the ribs and the bracing, while the prototypes used box sections for the ribs and box sections or standard rolled sections for the bracing.

From Column (1) of Table 2-1, it can be seen that the loads on the structure are directly related to the strength of the structure. Of the three basic construction materials to choose from, steel, aluminum, and plastic, aluminum was chosen. It provided more linear and less creep behavior than plastics, and required smaller loads than did steel.

Shown in Figure 2-1 is a schematic drawing of the model used.

2.4 Computer Analysis

Before construction of the actual model, a numerical solution for the linear elastic behavior of the arch bridge was obtained. The SAP IV (3) finite element program was used. The computer model simulated in every respect the physical model, except that between each pair of panel joints the arch ribs were approximated by two straight equal length beam elements, since SAP IV has no curved beam elements in its library. By considering single fold symmetry about the crown, only one half of the structure need be studied. The boundary conditions consisted of allowing the crown to displace vertically, laterally, and to twist about its longitudinal axis. At the support of each rib, only translations and axial twist were restrained. The axial twist was provided by adding a torsional boundary element at the end of each rib, and tangent

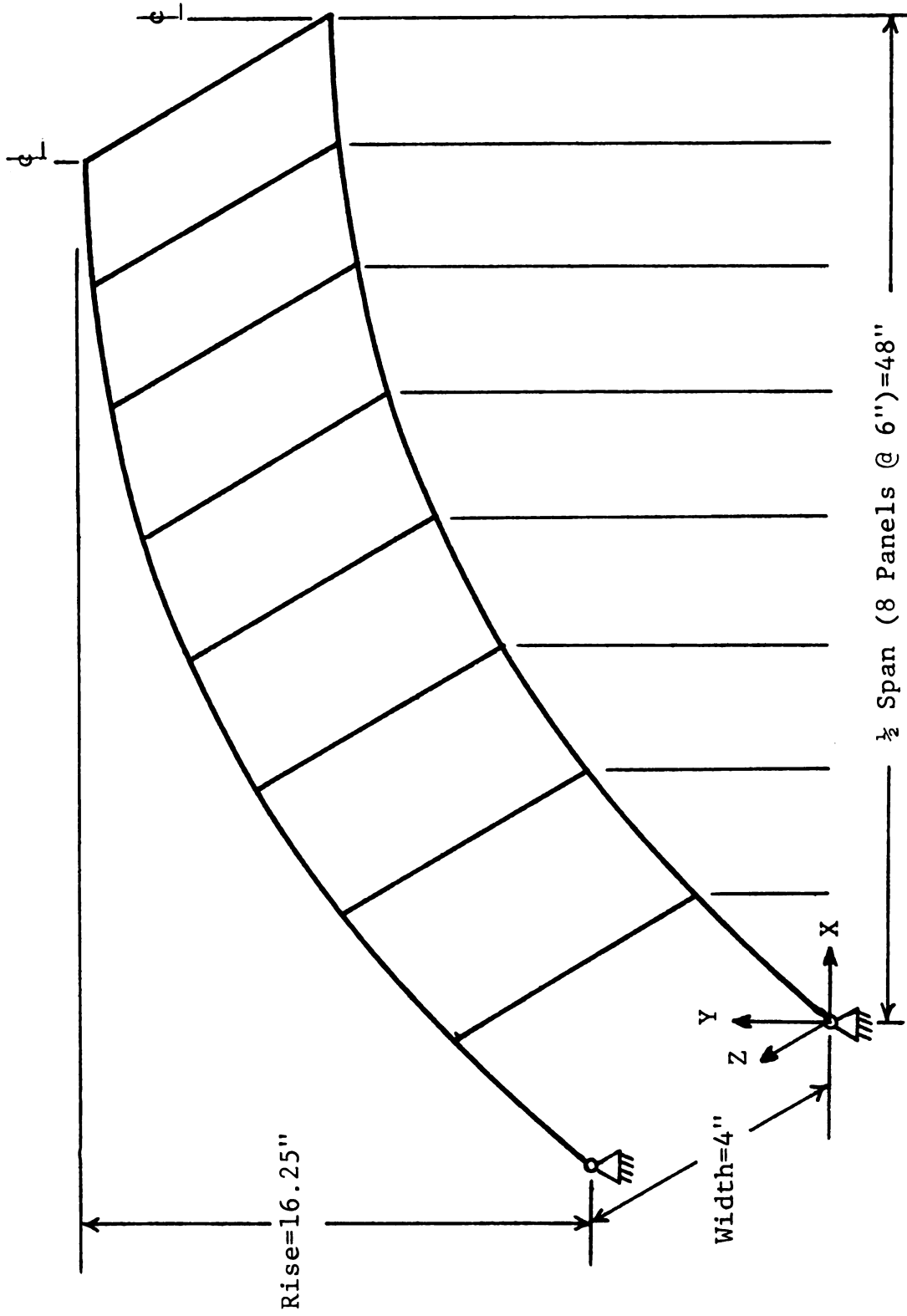


FIGURE 2-1 Arch Bridge Test Model.

to the rib slope at that point.

The computer solution indicated that when the model was subjected to a lateral loading (w) of 0.71 lbs./in., corresponding to a 100 m.p.h. wind, the lateral displacement at the crown would be 2.00 inches, giving a lateral stiffness (K_h) of 0.353 lbs./in.. It should be noted that since SAP IV is limited to linearly elastic structures, K_h is then independent of any vertical load applied to the model. Indeed, computer solutions by SAP IV cannot reflect nor predict any of the nonlinear behavior exhibited by the physical model. In this sense, the computer solution has only limited application to this study, which as will be shown later, was dominated by nonlinear behavior.

2.5 Test Apparatus and Construction

2.5.1 Arch Ribs and Bracing

Figures 2-2 & 3 show the arch bridge model. The ribs were cut from a single sheet of 2024-T3 aluminum with a reported Young's modulus of 10^7 psi, and a Poisson's ratio of 0.32. The value of Young's modulus was confirmed by a tension test performed on a sample coupon. The ribs were cut to shape, instead of being bent, to avoid the stresses of bending. The bracing, item (1) in Figure 2-4, were machined from a single bar of 2024-T3 aluminum. This figure also shows the connections used in attaching the bracing to the ribs. Holes were drilled through the ribs so that the panel "joint collars", item (B) in Figure 2-4, could be securely affixed with the bracing attached to the collar.

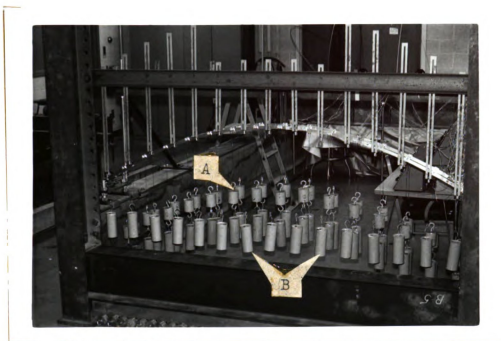


FIGURE 2-2 Side View of Bridge Model

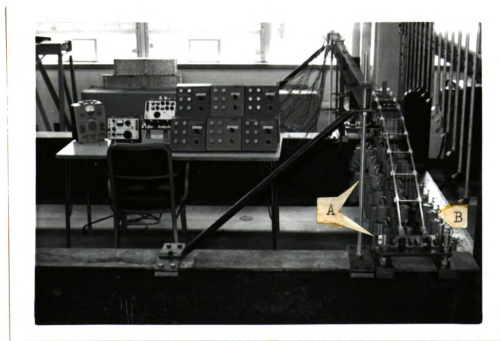


FIGURE 2-3 End View of Bridge Model

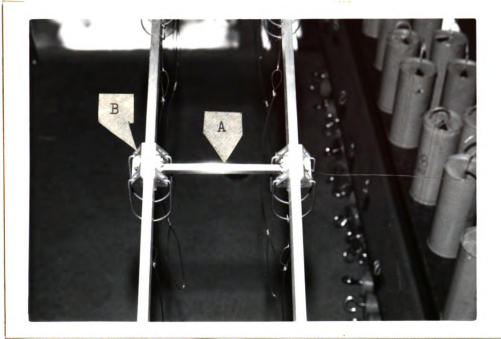


FIGURE 2-4 Bracing

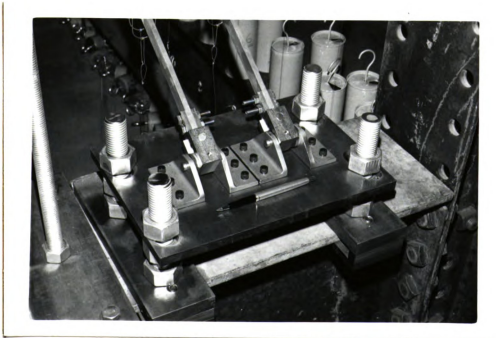


FIGURE 2-5 Hinges

2.5.2 End Support

Shown in Figure 2-5 is the end support assembly. The hinge assembly must satisfy the previously mentioned boundary conditions, and be able to provide a stable platform that will not displace during the course of testing.

The hinges were designed similar to a universal joint that is commonly used in automobile transmissions. The only displacements permitted were rotations about the two pins.

The base plates that held the two sets of hinges were leveled to within 1 mm of each other with the aid of a surveying theodolite.

2.5.3 Panel Joints

On the arch bridge, the panel joint is where the bracing and the deck hangers frame into the rib. Figure 2-6 shows a typical panel joint from below, the rib (A), bracing (B), and the load hangers (c). The load hangers were designed to orient the vertical loads through the center line of the rib before and after displacements. This is important since any misalignment of the loads could create an eccentricity which would give rise to moments that would alter the behavior of the bridge.

2.5.4 Loads

The loads that are applied to the structure are done so by using combinations of solid lead cylinders, and canisters containing various amounts of lead shots. The solid lead cylinders, which were used only for the vertical loads were formed in 16 oz. beer cans, and came in weights of about 3.50, 6.75, and 1.75 lbs. each. These cylinders had screw hooks



FIGURE 2-6 Panel Joints

attached at both ends so that several cylinders in combination could be connected to any given panel joint. The lead shot, 0.14 inch diameter balls, was held in separate canisters with a wire hook attached to the lid so that it too could be added in tandem with the solid cylinders. For ease of construction, the solid lead cylinders were not formed to an exact weight. Thus, the lead shot canisters were also used to equalize the vertical loads on the panel joints. The lead shot canisters were oriented so that their ring tab openings remained on top. This facilitated the addition of the lead shot load increments into the canister without having to take the canister off of the structure for loading which would disturb the system.

The lateral loads which simulated wind loads, were attached to the "leeward" rib of the bridge. Using monofilament nylon fishing line, the line was passed through a nylon pulley where the lateral load is transformed from the lead weights. Figures 2-2 & 3 show the vertical loads (A), and the lateral loads (B) in place.

2.5.5 Measurement Equipment

Four dial gages, whose least count were 0.0005 inches, were stationed along the bridge. From one support, the gages were located 9, 27, 48, and 69 inches, and the deflections measured were labeled, respectively, Δ_1 , Δ_2 , Δ_3 , and Δ'_2 , where Δ_3 corresponded to the crown, and Δ_2 and Δ'_2 were at about the quarter points. Hereinafter, they will be referred to as the quarter point displacements. With this arrangement of dial gages, the deformed behavior of the model

could be monitored.

III. TEST PROCEDURES

Two test programs were conducted: First, using the vertical loads only, and secondly, using both vertical and lateral loads. These tests are described in the following sections.

3.1 Vertical Load-Only Tests

As mentioned previously, the vertical loads which represent the dead load plus the live load were suspended from the panel joints. The panel loads were equal and the arches should essentially be in a state of uniform compression. In this test, at each vertical load level, the lateral displacements were, of course, due to the unavoidable imperfection in the system.

Initial tests indicated that in order to obtain meaningful results the changes in vertical loads must be monotonic. That is, alternate loading and unloading should be avoided. This required a programming of the loading procedure. Since the lead shot canisters were not large enough to hold the volume of lead needed for the maximum load required, it became necessary to use a "piece-wise-continuous" approach to the vertical loading. This approach consisted of applying a base load set to be equal to several load increments below the maximum load of the preceding series of tests, excepting, of course, the initial load segment for which the base load is

zero. Increments of lead shot were then added to the base load monotonically. With an overlapping of data points, it is then possible to coalesce the data so that it would represent the structural behavior under a monotonic loading.

In the course of developing the above test technique, it was found that the behavior of the model bridge was very sensitive to the way in which the vertical loads were applied to it. Care must be exercised to align the load to avoid eccentricities, to smoothly transfer the loads onto the model to avoid any impact loading, and it also became clear that the base loads could not usually be applied in a single step. The practice of adding the base loads in two or more steps was then adapted to correct the latter problem. The vertical base loads had to be applied in systematic manner to prevent the model from behaving erratically. These loads were applied in pairs, with two panel joints per station and then symmetrically about the crown, starting at the supports and working towards the crown.

The vertical load increments, consisted of 0.35 lbs. per canister of lead shot, were added in a similar manner as were the base loads, except that only one canister was incremented per side at a time. To avoid an unbalanced loading situation during the load incrementation process, the loads were simultaneously added to the panel joints that are symmetric with respect to the crown, but on different ribs.

3.2 Combined Lateral and Vertical-Load Tests

This set of tests were designed to evaluate the effects of the vertical loads upon the lateral stiffness of the

structure when subjected to simulated wind loads. This required, first, the establishment of a vertical load, as described previously, and secondly, a monotonically increasing series of lateral loads. Using the dial gage readings of the horizontal displacements measured from the tests, a family of load-displacement curves can be constructed to show the effects of the vertical load on the lateral stiffness.

The lateral load increments consisted of measured amounts of lead shot, weighing either 0.22, 0.11 or 0.06 lbs., added in a fashion, symmetric with respect to the crown, progressing from the support towards to the crown. The differences in the increments used was brought about by the change in responsiveness toward lateral displacements as the vertical loads were increased. When the vertical loads were small, the larger increments provided a good linear data spread. But with the larger vertical loads, smaller lateral load increments were required to produce similar results. When the lateral displacement reached about 0.75 inches, these tests were stopped in order to prevent any damage from occurring to the structure.

IV. RESULTS AND DISCUSSION

4.1 General

The results of this investigation will be presented in terms of both the overall behavior of the model and the behavior of the crown and for a point close to the quarter point for both loading systems employed. With the information obtained from the behaviors of the crown, estimates can be made of the buckling load of the model. Comparisons will then be made between the results obtained from this investigation to those of certain previous investigations.

4.2 Behavior Under Vertical Loads-Only

4.2.1 Overall Behavior

If one considers a simply supported beam-column, it is well-known that its first mode of buckling will appear as a half sine wave; this may be called the symmetric buckling mode. At an axial load four times larger than that required to cause the beam-column to buckle in the symmetric first mode, the second mode will appear. This mode appears as a full sine wave, and may be referred to as the antisymmetric buckling mode. Thus, in the case of a beam-column, the buckling loads corresponding to the symmetric and antisymmetric modes are quite distinct in the sense that the latter is four times the former. Indeed, for this reason, it has little engineering significance.

However, for arch bridges, this is not necessarily true. Due to the curvature of the structure and possibly the bracing, the antisymmetric mode may correspond to a lower load level than that for the symmetric mode. There also exists the possibility that the buckling loads corresponding to the two modes could be quite close to each other so that some form of interaction may occur prior to entry into either buckling mode as the loads are increased.

Shown in Figure 4-1 is the displaced shape of one rib of the bridge model for four typical vertical load tests. The dial gages were labeled Δ_1 , Δ_2 , Δ_3 , and Δ'_2 , and their locations have been given in Chapter II. It is shown that the model appears to be deforming in a manner that is a combination of a symmetric and antisymmetric modes. If the deformation was antisymmetric, there should be no displacement at the crown, and if it were symmetric, Δ'_2 should not have the opposite sign of Δ_2 (at mirror point of Δ'_2 , and Δ_3 should be greater than Δ'_2). Since the model was not tested to actual collapse, the exact nature of the final failure mode is not known.

It can be speculated that the appearance of the combination of the two modes could be the result of (A) that the initial imperfection (eccentricities) contains substantial components in both modes and (B) that the critical loads for the modes are close to each other.

4.2.2 Crown Behavior

If the symmetric mode was the mode of failure for the model, a study of the behavior of the crown could enable one

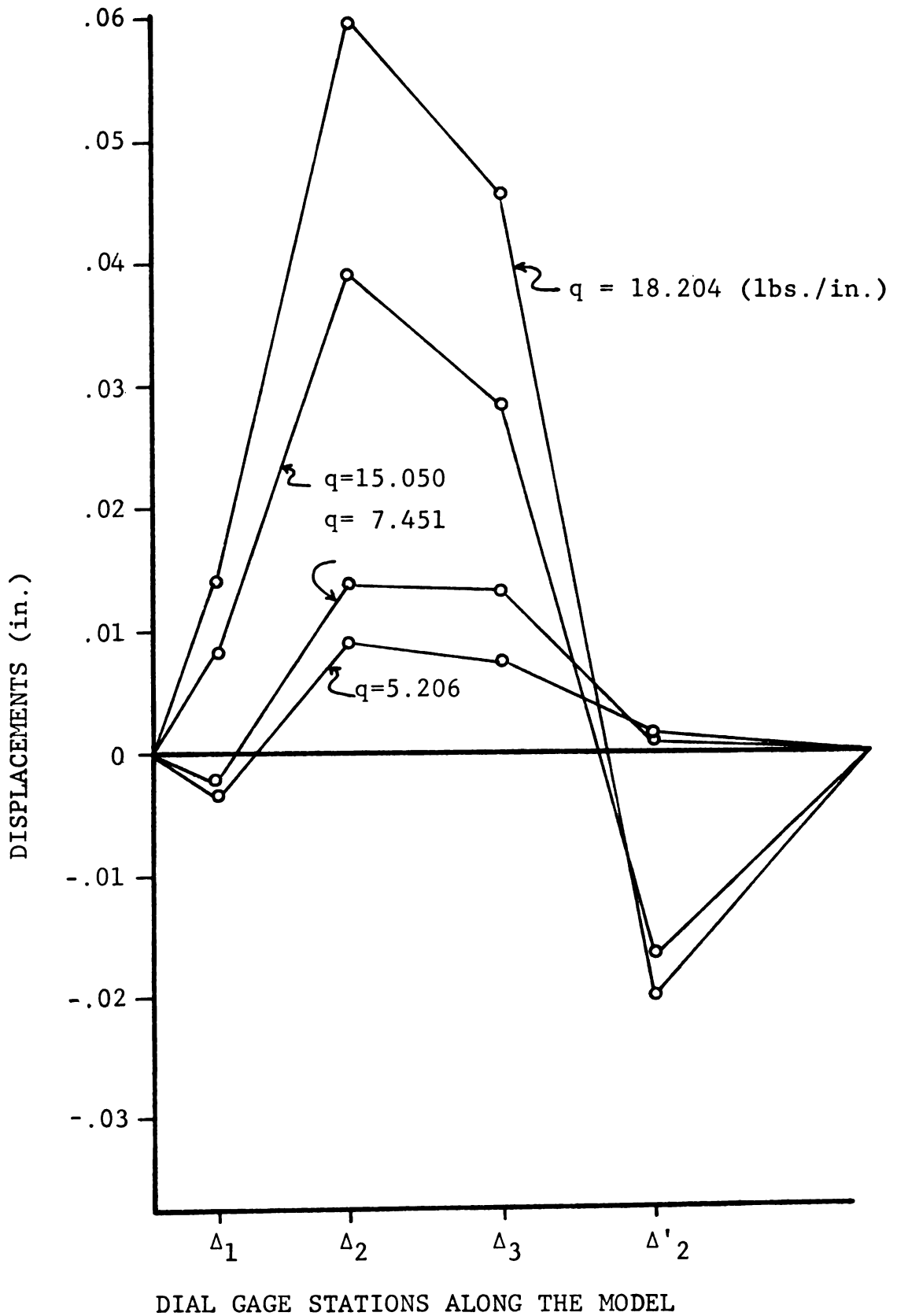


FIGURE 4-1 Displaced Shape of the One Rib under Typical Vertical Load-Only Tests.

to predict the critical buckling load. Should a structure be perfectly built and loaded such that there are no eccentricities, it could be deformed without the occurrence of buckling. There could be no lateral displacement due to vertical loads alone. But every structure contains some degree of initial imperfection. This could be in the form of members not being straight, the structure not being plumb, play in the connections, or the loads may be applied with eccentricities.

As the loads are gradually increased, a linear relationship will develop between the applied loads and the lateral displacements. After a certain level of loading has been reached, all subsequent loads would have a nonlinear relationship to the lateral displacement, with each equal load increment creating successively larger displacement increments. It is this nonlinear behavior that reduces the overall stiffness of the structure. When the stiffness is reduced to zero, the structure is said to have buckled.

Shown in Figure 4-2 is a plot of the vertical load versus lateral displacement at the crown. The data points form a smooth curve, with the exception of the first four points. The deviation of these four points from the expected path, is probably due to the fact that the structure was in the process of adjusting to the initial slacks existing in the various joints and hinges. After the structure has "removed the slacks", it can be seen that a linear region extends to about 2.0 lbs./in.. Beyond 2.0 lbs./in., the structure progresses into a nonlinear range.

The distribution of data points is seen to be quite

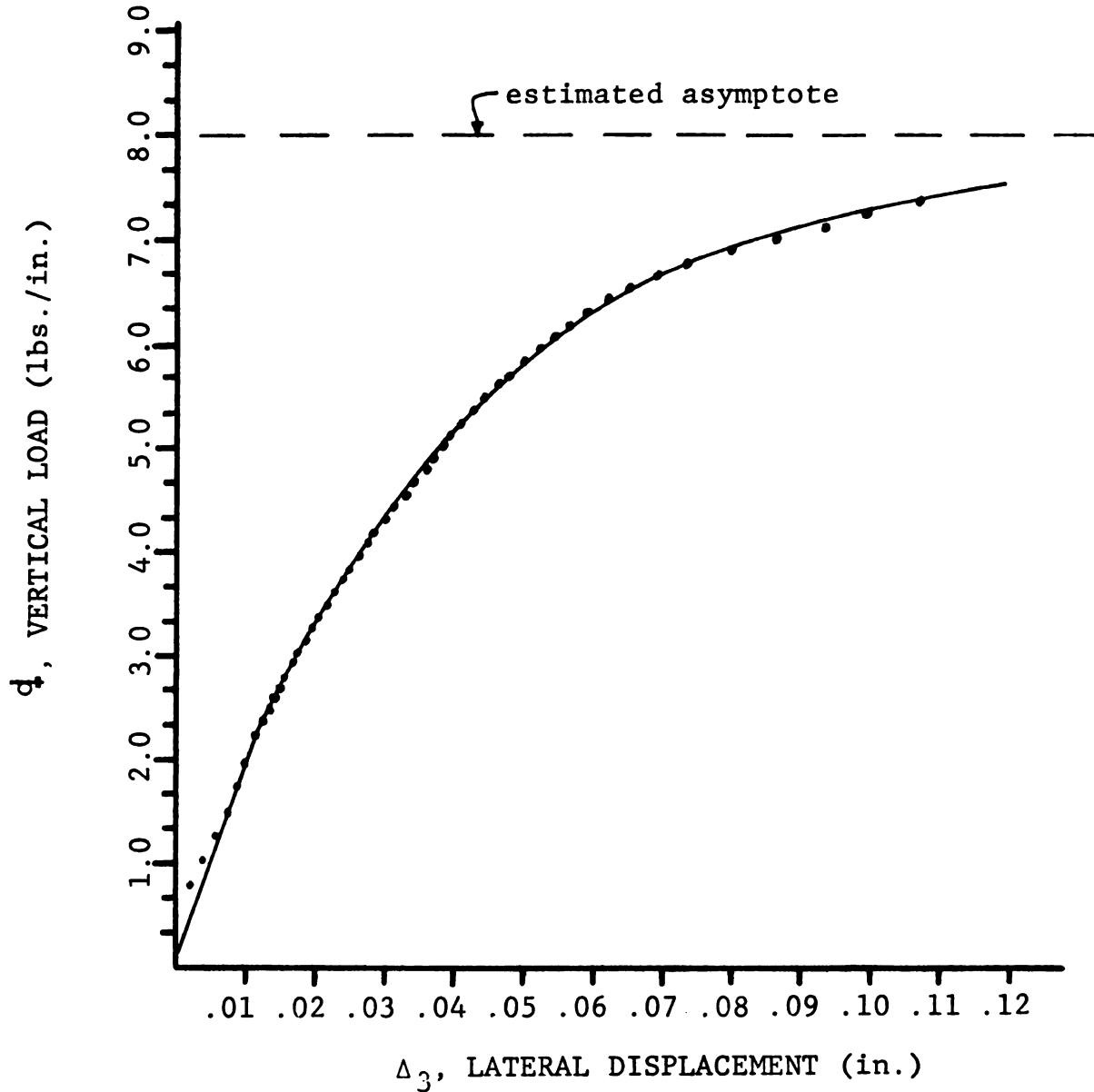


FIGURE 4-2 Load-Displacement Curve For The Crown Under Vertical Loads-Only

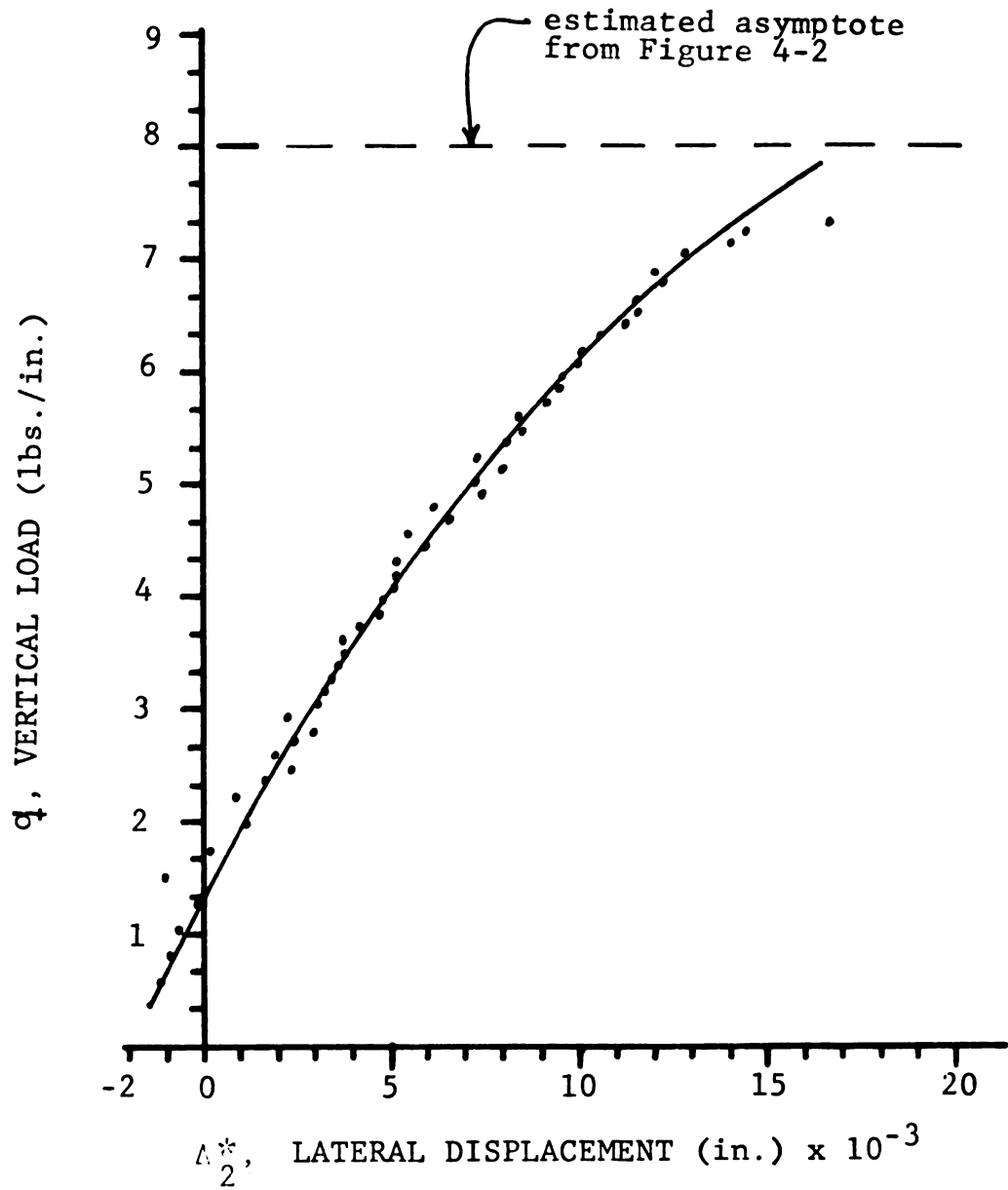


FIGURE 4-3 Load Displacement Plot For The Antisymmetric Component of Δ_2

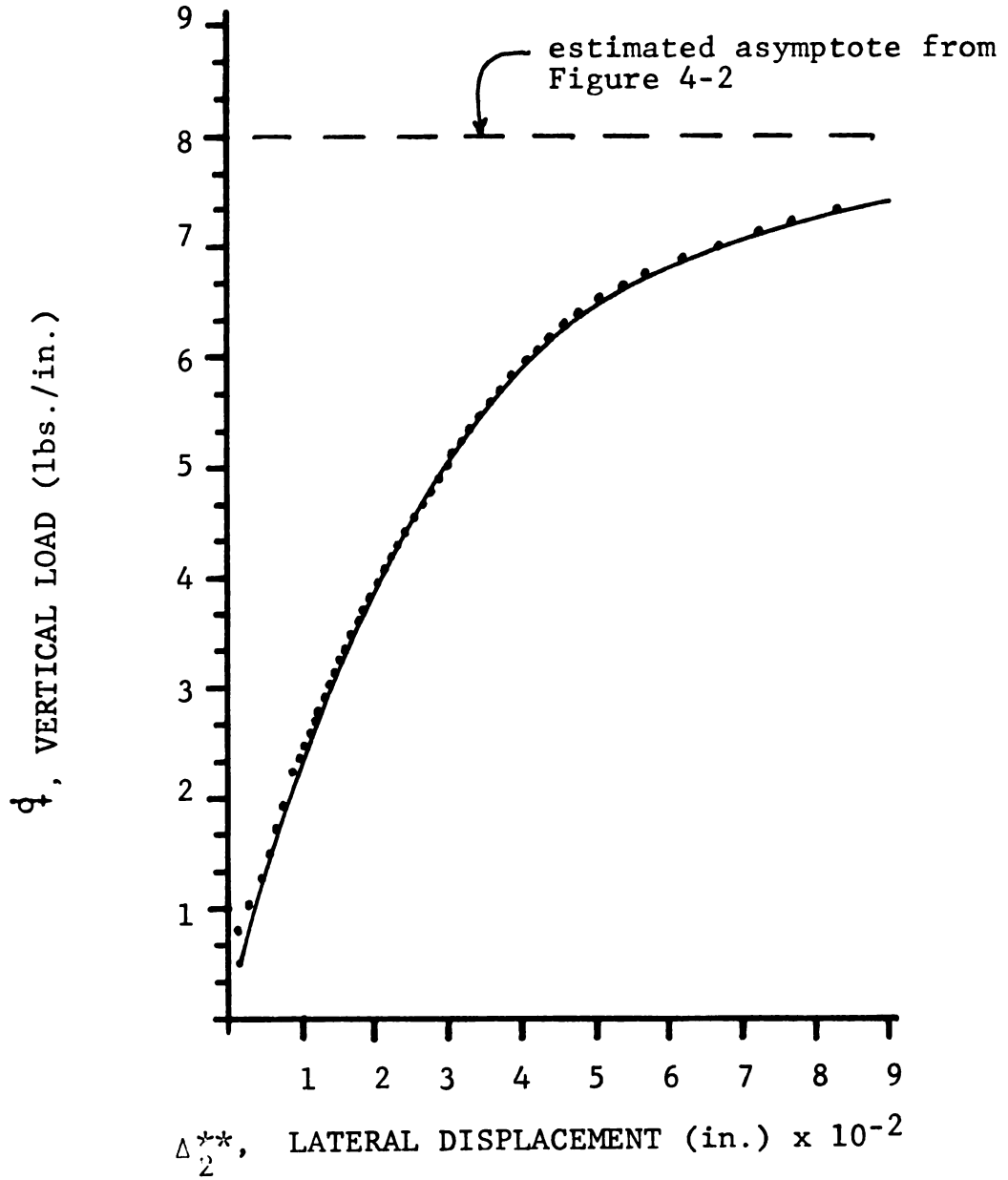


FIGURE 4-4 Load-Displacement Plot For The Symmetric Component of Δ_2

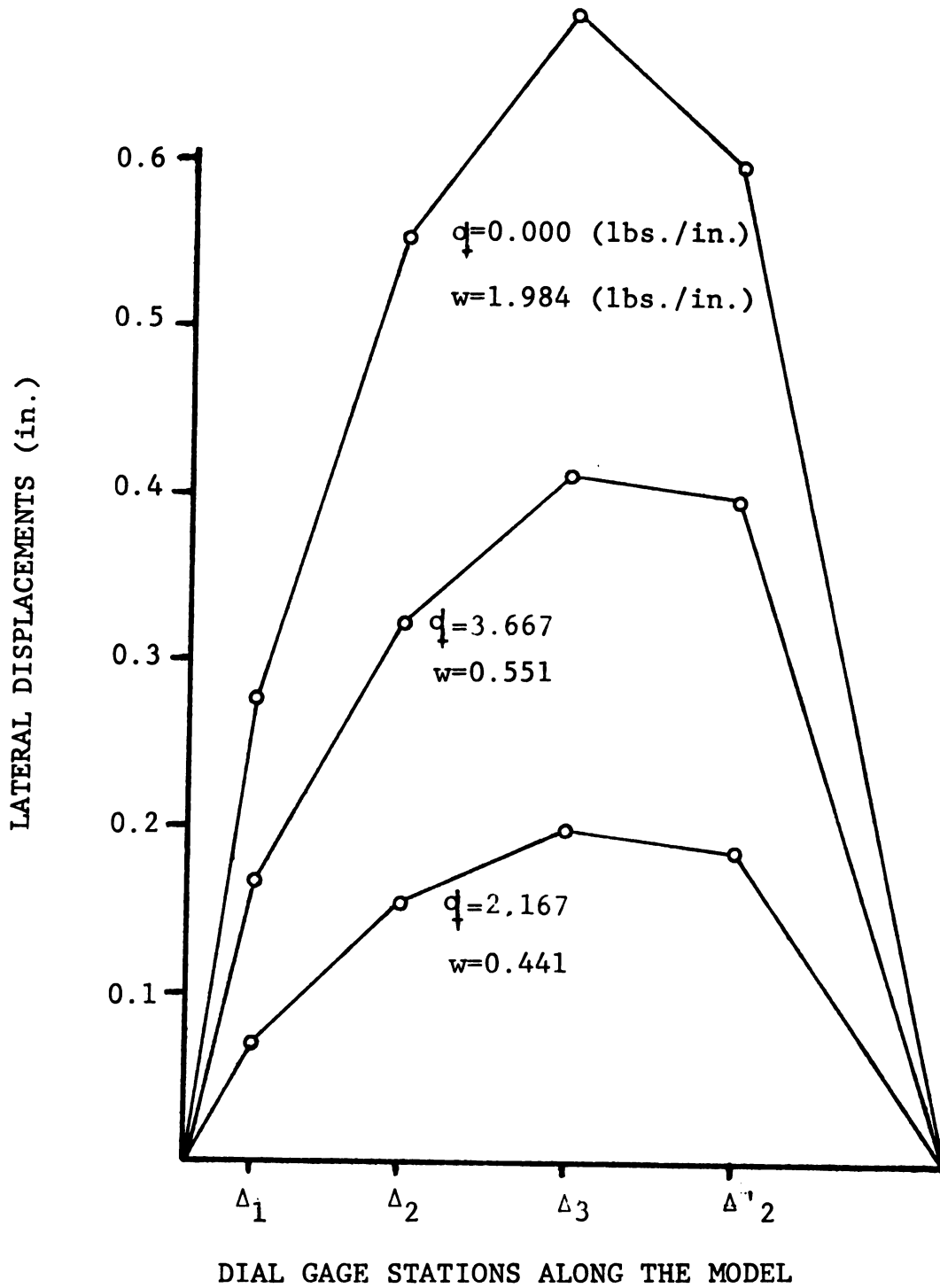


FIGURE 4-5 Displaced Shape of One Rib Under Typical Combined Load Tests

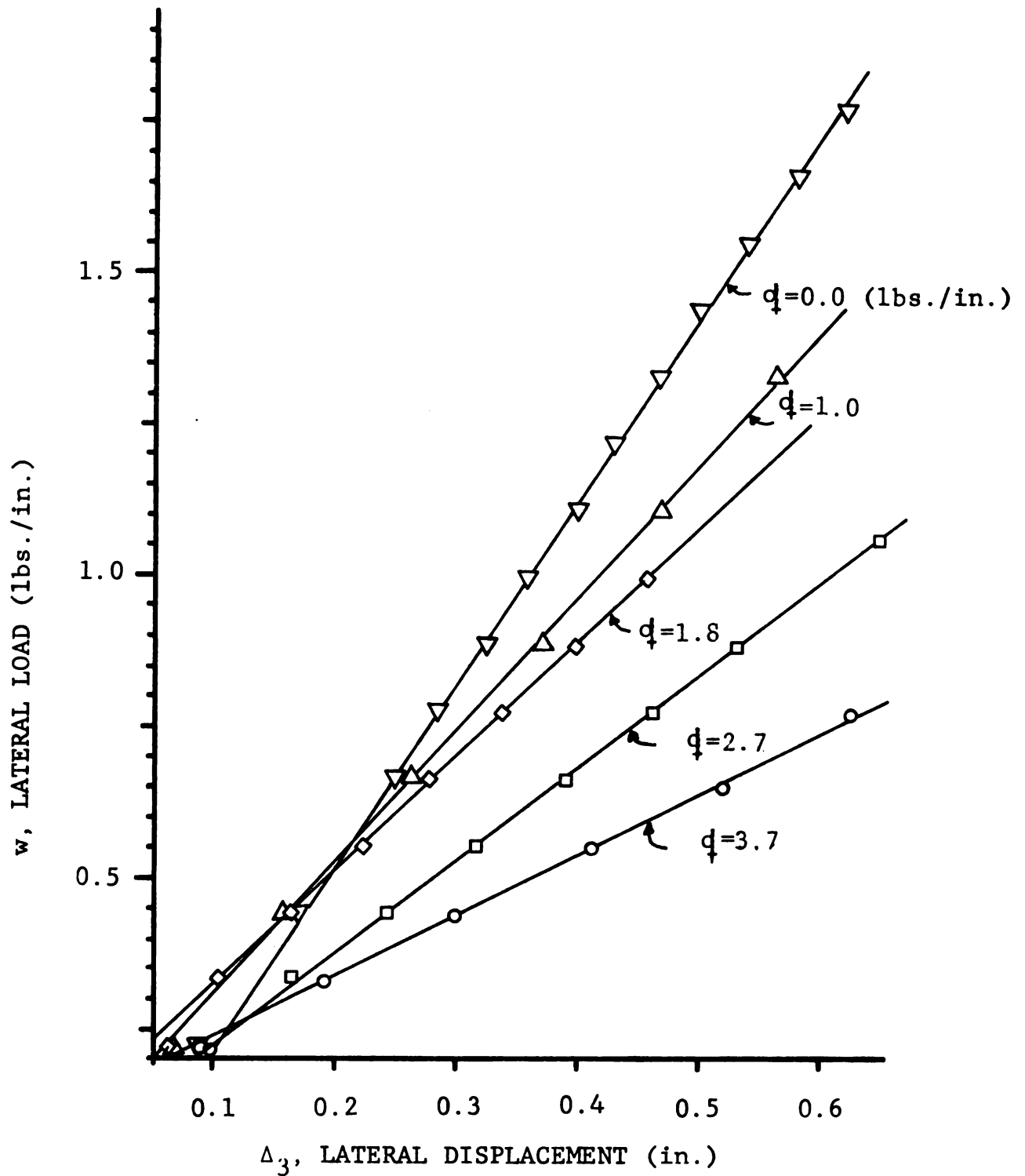


FIGURE 4-6 Load-Displacement Plots For The Crown
Under Combined Load Tests
($q=0.0, 1.0, 1.8, 2.7, 3.7$)

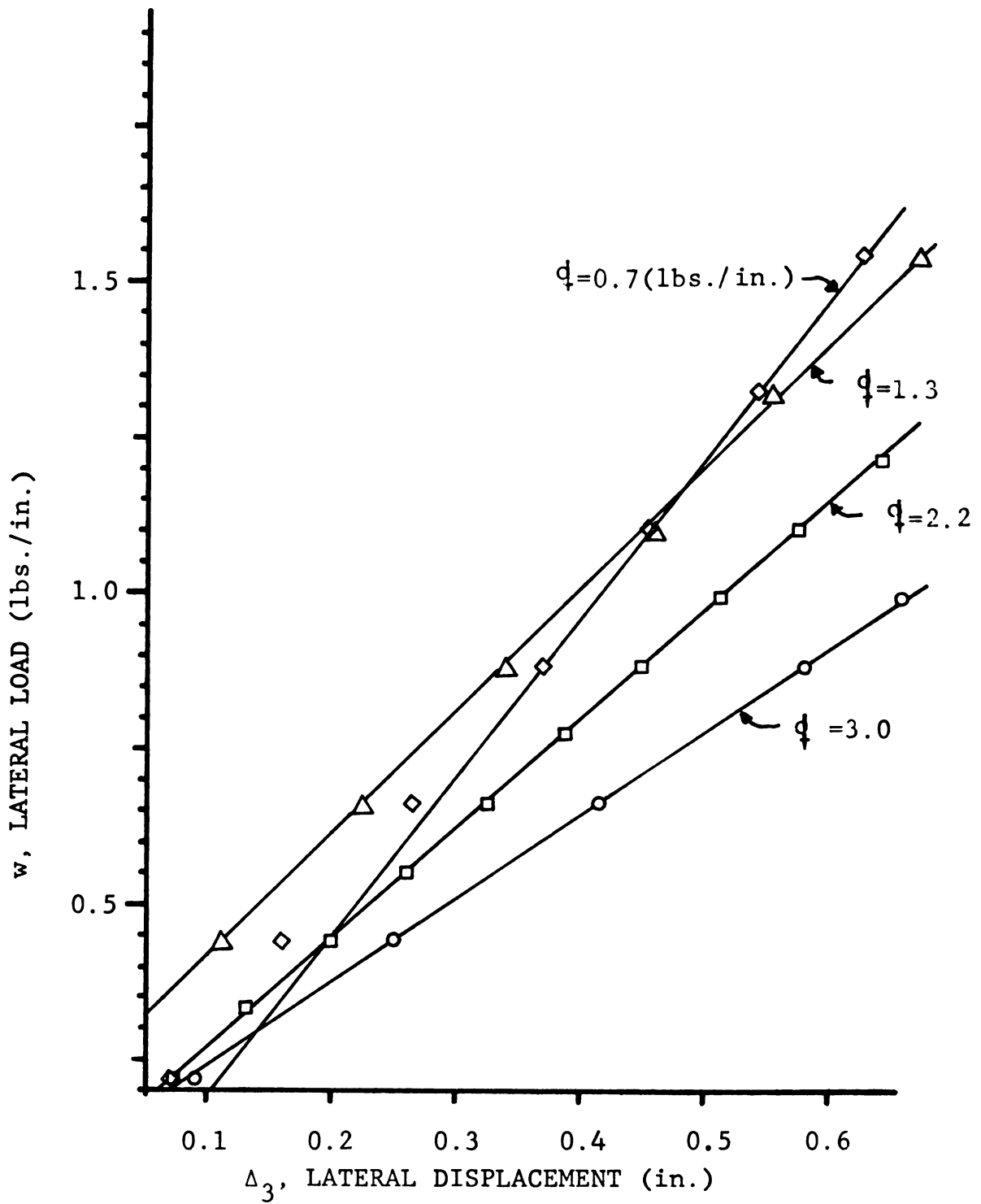


FIGURE 4-7 Load-Displacement Plots For The Crown
Under Combined Load Tests

($q=0.7, 1.3, 2.2, 3.0$)

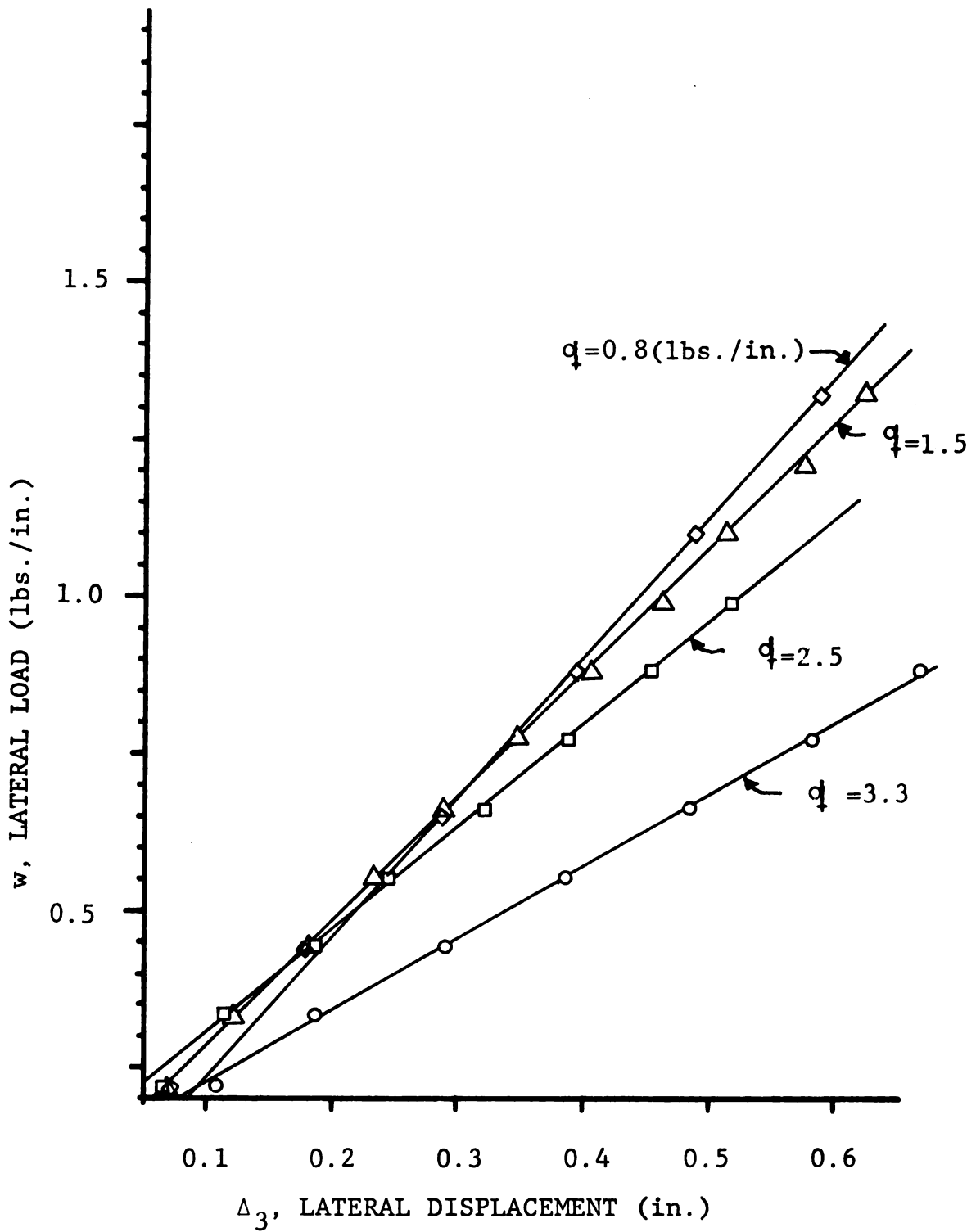


FIGURE 4-8 Load-Displacement Plots For the Crown Under Combined Loads

($q=0.8, 1.5, 2.5, 3.3$)

smooth which seems to justify the use of the segmented testing procedure that was discussed in the preceding Chapter. An extrapolation of this curve could lead to an estimate of the buckling load which will be discussed later.

4.2.3 Quarter Point Behavior

Since the displaced form of the arch bridge ribs appears to be a combination of the symmetric and antisymmetric modes, the behavior of the quarter point should be investigated. If the displacements are a combination of the two predominant modes, their components could be separated. The following formulas were used to extract the two mode components:

$$\Delta_2^{**} = \Delta_3 \sin\left(\frac{\pi X}{L}\right) = (0.773) \Delta_3 \doteq \text{Symmetric Component}$$

$$\Delta_2^* = \Delta_2 - \Delta_2^{**} \doteq \text{Antisymmetric Component}$$

Presented in Figures 4-3 & 4 are the load-displacement plots of the extracted antisymmetric and symmetric components of Δ_2 respectively. The general behavior can be seen to resemble that of Figure 4-2, Figure 4-4 more so than Figure 4-3. With these plots, additional estimates of the buckling loads can be made.

4.3 Behavior Under Combined Lateral and Vertical Loads

4.3.1 Overall Behavior

If one was to observe the horizontal projection of the deformed bridge subjected to lateral loads, it could be seen that the model would behave in a manner similar to that of a simply supported beam carrying a uniformly distributed load. In Figure 4-5, the generally symmetric shape of the deformed

bridge can be seen for typical tests using a combination of vertical and lateral loads.

It was noted in testing, that there also existed a need for an initializing lateral load for the model to adjust to the slack in the system in addition to the vertical initializing load mentioned previously. Beyond this initializing load, the structure would behave linearly. The magnitudes of the displacement measured, as shown in Figure 4-5, are an order-of-magnitude larger than those that appear in Figure 4-1 for vertical loads alone. This would mean that factors such as imperfections and internal friction would have a smaller influence on the behavior under horizontal loads than that on the behavior under vertical loads only.

4.3.2 Crown Behavior

Presented in Figures 4-6, 7 & 8 are plots of the lateral displacement versus lateral loads for given levels of vertical loads. It can be seen that for each of the vertical loads, there existed an essentially linear relationship between lateral displacement and the load. However, such results were unobtainable for vertical loads of 4.0 lbs./in., and greater, since upon application of the lateral load required to remove the initial slack, the structure seemed to be already in a state of impending collapse; i.e., no linear range of the load-displacement relation could be obtained.

In Figures 4-6, 7 & 8, the slopes of the lines represent the lateral stiffness of the bridge at different levels of vertical loading. Plotted in Figure 4-9 are these stiffnesses versus vertical load level. It can be seen that as the

vertical load was increased, the lateral stiffness of the structure decreased. When the stiffness decreases to zero, buckling is said to take place. This will be discussed in the following section.

4.4 Buckling Load

The results presented in this section are separated into two parts: Firstly, the results derived from the vertical load only testing and, secondly, the results obtained from the combined loading.

4.4.1 Vertical Load-Only

As mentioned previously, buckling occurs when the stiffness of the structure is reduced to zero. When this happens, no further load increment is required to provide additional displacements. From Figure 4-2, the point of zero stiffness can be located by finding the asymptote of the load-displacement curve. The asymptote was estimated, by eye, to be about 8.0 lbs./in.. This approach, however, only holds if the buckling mode is of the symmetric type.

In Figures 4-3 & 4, the plots of vertical load versus lateral displacements for Δ_2^* and Δ_2^{**} can be seen. Since these displacements occur close to the one-quarter point, they could be used to evaluate the antisymmetric mode. The asymptote for the extracted symmetric mode is about 8.0 lbs./in.. No estimate is possible for the extracted antisymmetric mode since the curve has not leveled off noticeably.

By using the data from Figures 4-2, 3 & 4, it is possible to construct the "Southwell plots" (6) for another estimation of the buckling load. The Southwell plot consists of plotting

Δ/q versus Δ . Figures 4-10, 11 & 12 present the Southwell plots for Δ_3 , Δ_2^* and Δ_2^{**} respectively. Normally, the Southwell plot would yield a single straight line, the inverse of whose slope would be equal to the buckling load. However, in Figure 4-10 two distinctly different straight line segments are seen. The corresponding values of the estimated buckling loads from Figure 4-10 are, 11.80 and 9.17 lbs./in.. From Figures 4-11 & 12, the estimated buckling loads of the symmetric and antisymmetric modes are 11.14 and 11.34 lbs./in., respectively.

4.4.2 Combined Load Testing

Another way to determine the buckling load is to determine the vertical load at which the stiffness under the application of lateral loads is zero; that is, where the curve representing the data points of Figure 4-9 will intersect the axis. The nature of the distribution of the data points is such that they seem to allow for more than one curve to fit. Therefore, two curves will be given here; first, a linear regression line, Line A, then a quadratic regression line, Line B. These can be seen in Figure 4-9 along with the SAP IV solution for the lateral stiffness that was described in Chapter 2. The latter solution agrees with the experimental data reasonably well at zero vertical load. But such analytical result based on a linear model is meaningless in the presence of substantial vertical loads.

The values of the buckling loads yielded by lines A and B are 5.59 and 6.73 lbs./in., respectively.

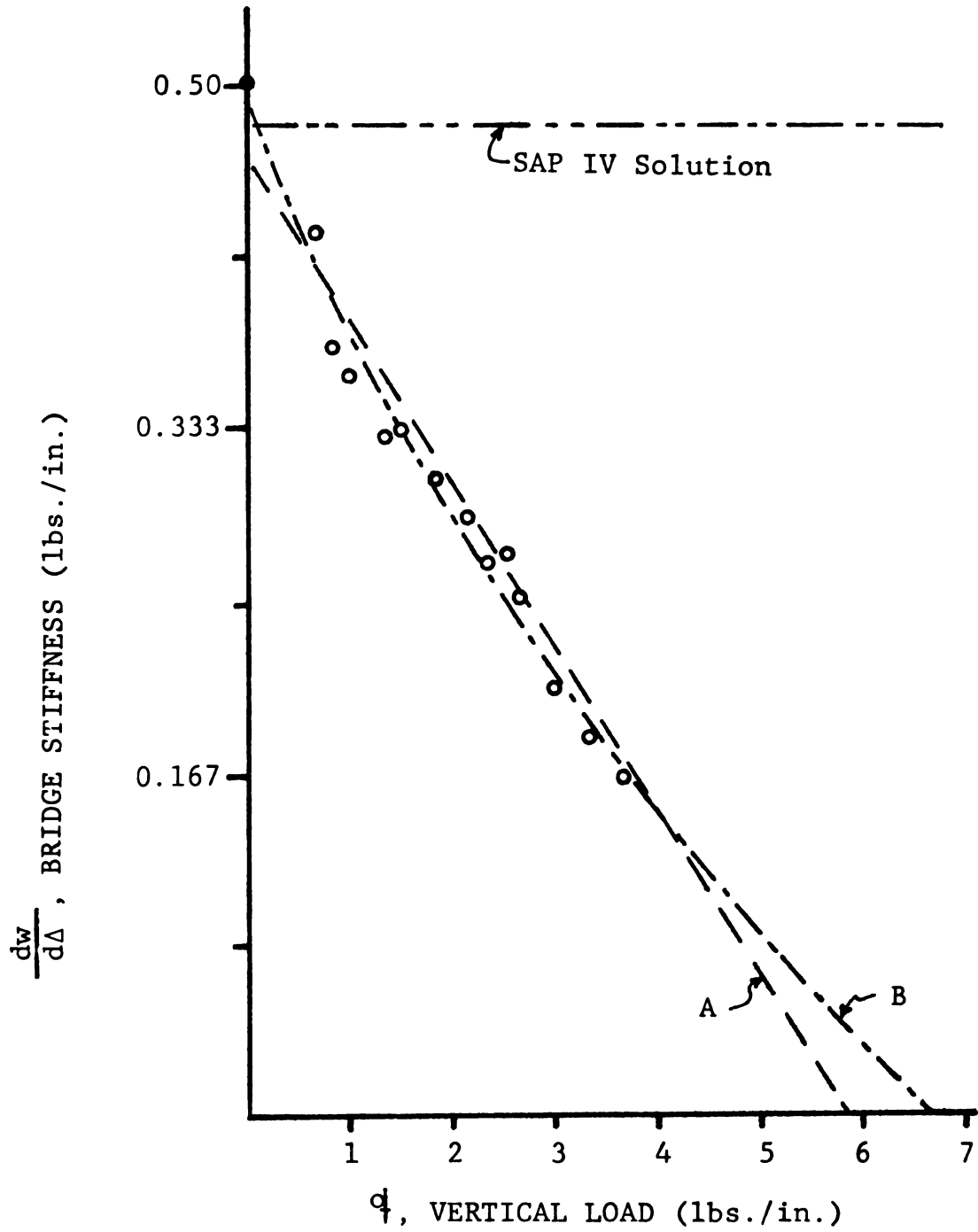


FIGURE 4-9 Lateral Stiffness versus
Vertical Load

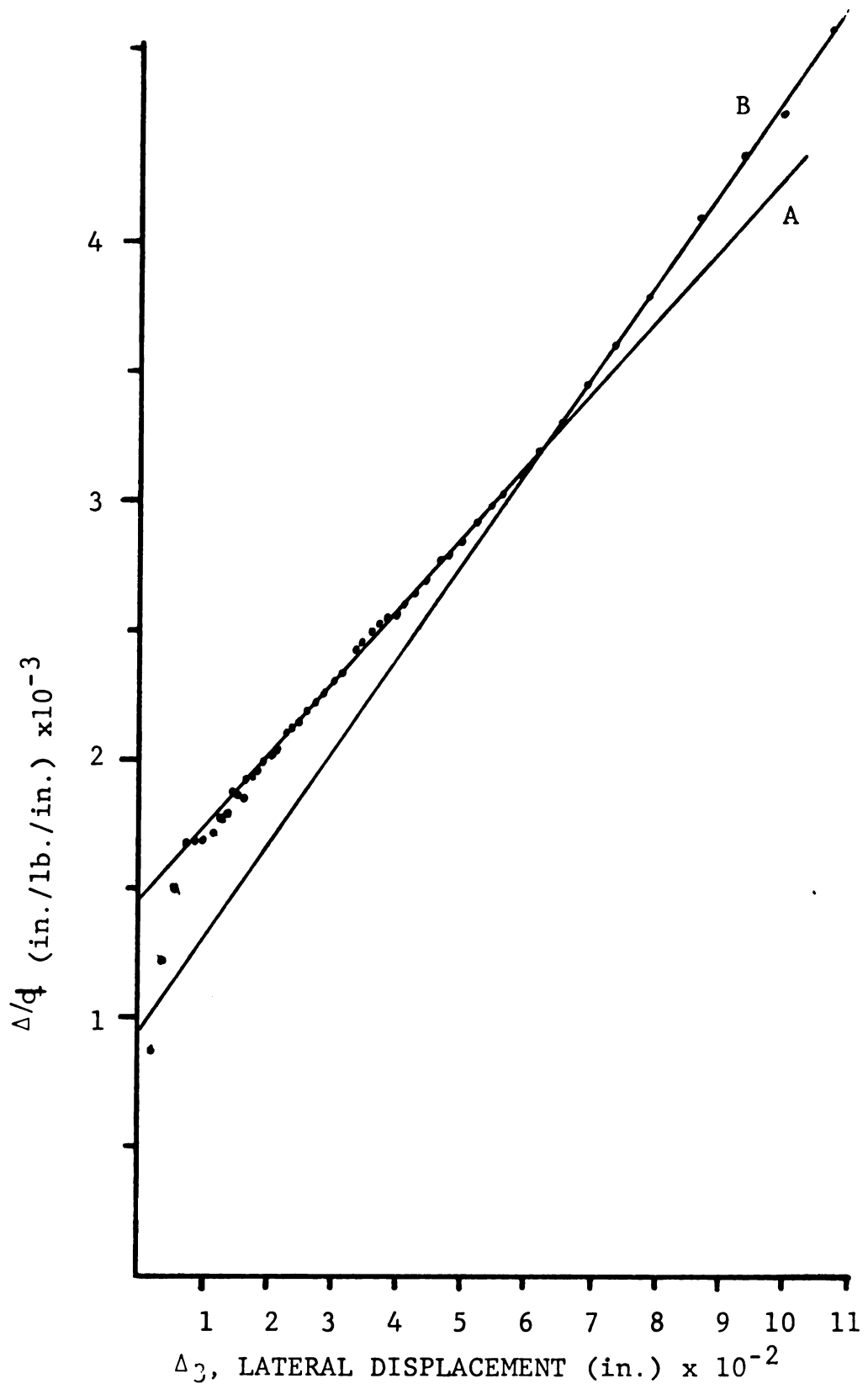


FIGURE 4-10 Southwell Plot For the Crown

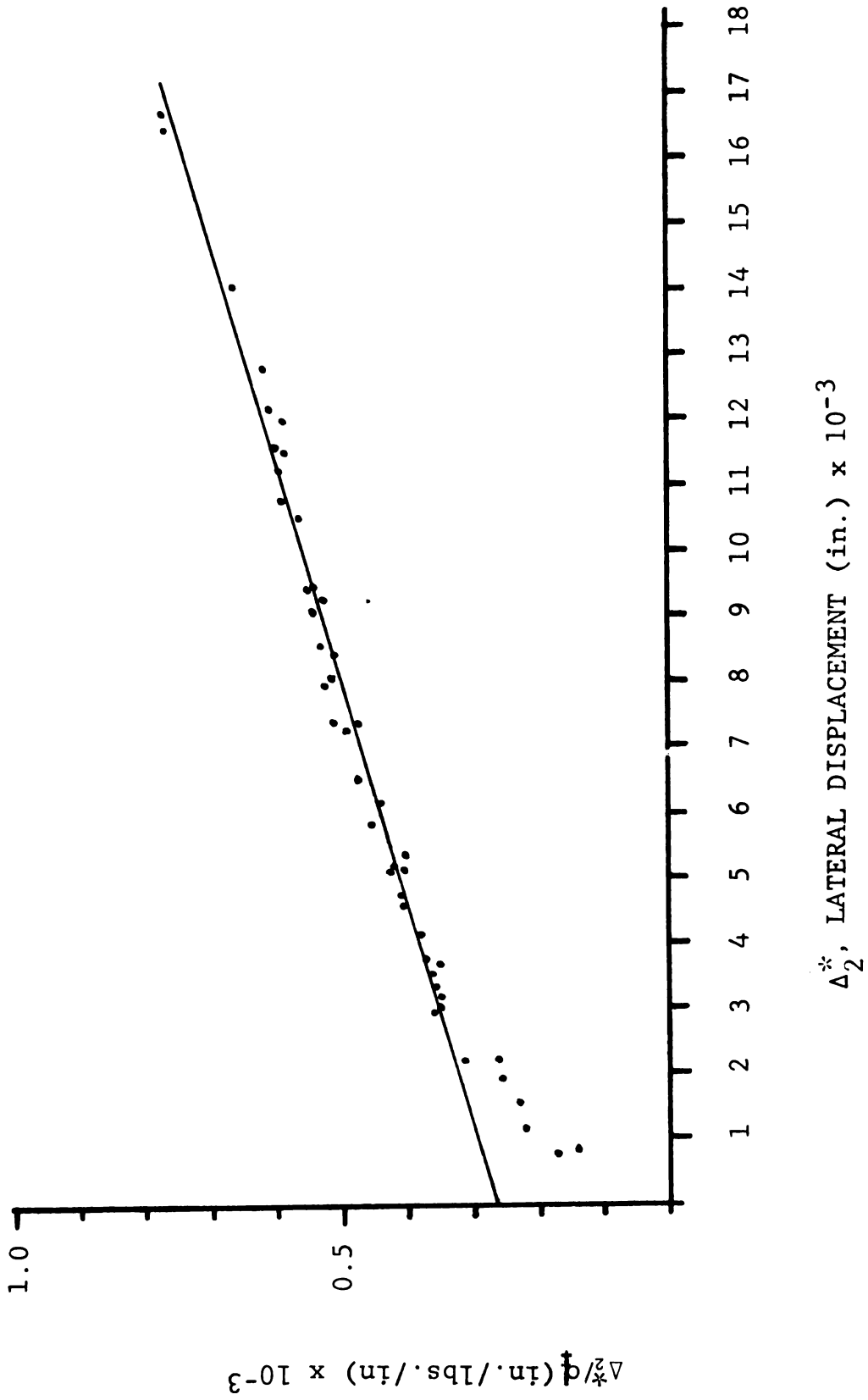
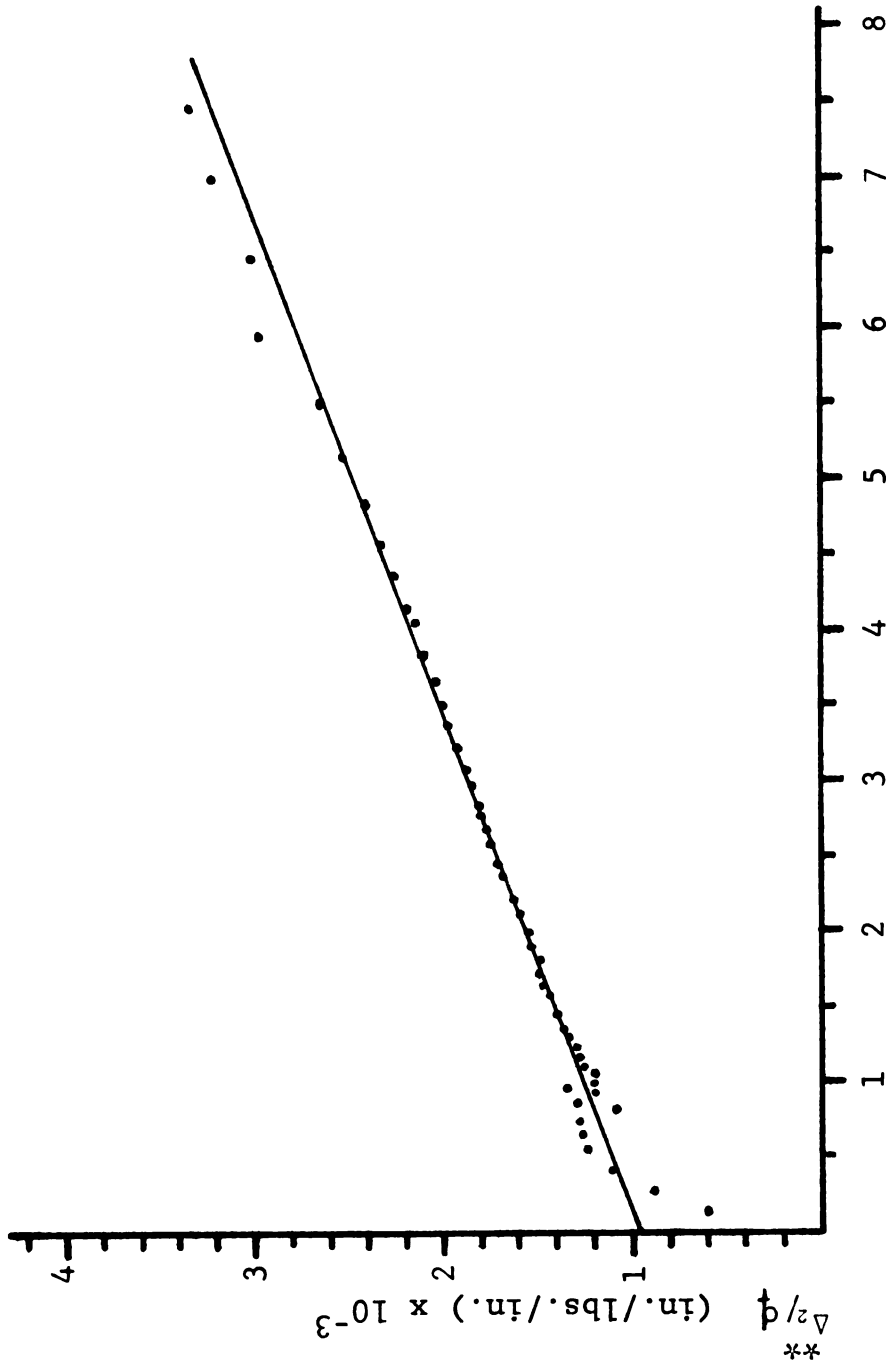


FIGURE 4-11 Southwell Plot For The Antisymmetric Component of Δ_2



**
 Δ_2 , LATERAL DISPLACEMENT (in.) $\times 10^{-2}$

FIGURE 4-12, Southwell Plot For The Symmetric Component of Δ_2

4.5 Discussion

A discussion of the results presented above will be divided into two parts; First, a discussion of the differences amount the results themselves, and secondly, a comparison of the results of the results of this investigation to those of previous investigations.

4.5.1 Differences Among Test Results

In Table 4-1, the values of the buckling load as obtained from the various interpretations of the experimental results given in the preceding section are tabulated. First of all, it should be noted that since the bridge was actually loaded to 7.36 lbs./in., without buckling, the buckling load must be larger than that. Thus, the values obtained from Figure 4-9, do not reflect the correct buckling load. But this does not mean that the method used to compute them is incorrect. The data points in the higher vertical load range which could not be obtained might indicate a flaring out of the curve which would indicate a larger value of the buckling load than extrapolated.

The double straight line feature of the Southwell plot in Figure 4-10 can perhaps be explained with the help of the dual mode displacement pattern indicated in Figure 4-1. The Southwell plot shifts from a higher buckling load to a lower one. Thus, Figures 4-1 & 10 seem to indicate that the structure started out in the antisymmetric mode, and remained in this mode until the changes in geometry allowed the symmetric mode to dominate, presumably to final failure. This behaviour may be interpreted from Figure 4-1 which shows that

TABLE 4-1 Tabulation of Experimental Buckling Load

<u>Estimation Basis</u>	<u>qcr (lbs./in.)</u>
Minimum	7.36
Asymptotic	
Symmetric (Δ_3)	8.00
Symmetric (Δ_2^{**})	8.00
Antisymmetric (Δ_2^*)	----
Southwell Plot	
Symmetric (Δ_3)	9.17/11.80
Symmetric (Δ_2^{**})	11.14
Antisymmetric (Δ_2^*)	11.34
Lateral Stiffness (K_h)	6.73

at the higher load levels, the rates of deformations are larger at the crown (representing the symmetric mode) than that of Δ_2 (representing the antisymmetric mode).

The Southwell plots produced from the extracted modes of Δ_2 indicate that, first, the buckling load in the antisymmetric mode is larger than that in the symmetric mode, and secondly, the two buckling loads are very close in magnitude. The buckling loads of the extracted modes by the Southwell plot method are larger than the buckling load estimates by the asymptote estimation. It would also seem that the true buckling load for the symmetric mode is closer to 8 to 9 lbs./in., that it is to 11 lbs./in., since the former value was indicated by more than one interpretation.

It should be noted that the buckling loads as deduced from Figures 4-2, 3 & 4, by the asymptote approach are subject to appreciable uncertainty. Since to avoid damaging the model, not enough data points were obtained to clearly delineate an asymptote. The asymptotes of the load-displacement curves for the crown (Δ_3) and the quarter point (Δ_2^*) show close agreement as to the magnitude of the buckling load of the symmetric mode. The asymptote for the antisymmetric quarter point (Δ_2^{**}) could not be determined, but the curve itself did show an asymptote representing a larger value than the symmetric mode buckling load.

4.5.2 Comparisons With the Results of Others

There have been relatively few studies performed on arch bridges. That is, a study of structural system of two ribs and a pattern of bracing that forms either a space frame or a space truss. On the other hand, the behavior of a single rib

has been studied quite extensively for almost any shape both analytically and experimentally, for example see References (2) and (3). This section will first look at a study by Shukla & Ojalvo (3) on single arch ribs in order to get a feel for the increase in stiffness generated by the addition of a particular bracing system. Then, a more detailed comparison will be made with a study performed by Tokarz (4) on parabolic arch bridges with a similar bracing pattern as employed in this investigation.

In the study by Shukla & Ojalvo, the major difference in the models used is in the application of the vertical loads. They assume that the deck system has infinite stiffness in the lateral direction. This would cause the vertical loads to tilt as the bridge deforms laterally. Thus causing a horizontal force component which tends to restrain the rib from buckling, and thus increase the buckling load of the system. Applying their results to only the arch rib of this investigation, the buckling load is calculated to be 1.21 lbs./in. of rib. Neglecting the differences in the models and loading, it would appear that the addition of the bracing used in this investigation would increase the buckling load by at least $3\frac{1}{2}$ times.

Before a meaningful comparison can be made with the results of the study by Tokarz, it is necessary to first examine the differences in the experimental models. Listed in Table 2-1, along with the values of the dimensionless variables used in this investigation, are the values used in the model by Tokarz. It can be seen that while most of the values

used in this study lie well within the computed range of realistic bridges, only a few values of the parameters of Tokarz's model did.

A number of differences appeared that could have a noticeable effect on any comparisons made between the two studies. First, it can be seen that the ratios of minor to major axis moments of inertia (I_{yy}/I_{xx}) and the polar to minor axis moments of inertia (J/I_{yy}) used in this study are, respectively, 7.28 and 9.23 times larger than those used by Tokarz. Secondly, the ratios of the minor axis moments of inertia between the bracing and the ribs (\bar{I}_{yy}/I_{yy}) used in this investigation are 241.7 times larger than those used by Tokarz. Neither his value, or the value used in this investigation managed to satisfy the range of real bridges. These differences are due mainly to his use of a deep thin rib (1.5 x 0.192 inches).

Another noticeable, and possibly important, difference is in the width to span ratios (h/L). Tokarz's value is 3.25 times larger than that employed in this study, and just larger than the range of real bridges. His models width is 8.0 inches (compared to 4.0 in.) and a length of 59.0 inches (compared to 96.0 in.). Considering the geometry of the structures alone, his model being shorter and wider should be more stable of the two. Unfortunately, the closest value of the buckling load that could be estimated from his data would be for an arch bridge with the value of KL/EI_{yy} , in which K is the flexural stiffness of the bracing ($6\bar{E} \bar{I}_{yy}/\bar{L}$), equal to $\frac{1}{32}$ of that used in this investigation.

The estimated buckling load thus estimated is 2.44 lbs./in.. This value is at least 3.3 times smaller than what has been computed for this investigation. Tokarz noted that the buckled shape of his model corresponded to the symmetric mode.

It should be noted that Tokarz also used the Southwell plot to determine the buckling loads from his test results. The displacements that were measured in his experiments were an order of magnitude larger than those recorded in this investigation. This, of course, is due to the fact that his model is less realistic as compared to that used in this study.

Even though no direct comparisons can be made between these experiments, it has been shown that, first, the addition of a bracing system will cause a noticeable increase in the stability of a pair of arch ribs, and secondly, that the stiffness in the minor axis direction of both the bracing and the arch ribs can significantly alter the stability of the arch bridge.

V. CONCLUSION

An experimental study of the nonlinear behavior of a parabolic arch bridge model, up to the point of buckling, is reported. The bridge model is 96 inches long, has a rise of $16\frac{1}{2}$ inches, and the ribs are 4 inches center to center.

Vertical and lateral loads were applied in various combinations to simulate actual load conditions. By applying the load increments in a monotonic manner, the behavior of the bridge could be observed and measured.

It was found that the symmetric and antisymmetric buckling modes are in close proximity of each other, but that the symmetric mode appears to be the failure mode. Several techniques were used to deduce the buckling load, and the asymptote and Southwell plot worked very well for both modes.

The decrease of the lateral stiffness due to vertical loads was also studied. However, the buckling load extrapolated from these results appears to be too low.

It should be noted, however, that this is only a preliminary study based upon a single bracing pattern and rib configurations. Further studies could be performed upon models with variations in parameters of rise to span ratios, end supports, bridge widths, and alternate bracing patterns. In particular, studies involving the K and X bracing patterns would be most desirable. The results obtained from such

analysis can be used not only for prototype bridges, but also for verification of analytical or numerical procedures needed for a general method for the design for stability in arch bridges.

LIST OF REFERENCES

LIST OF REFERENCES

- 1) Langhaar, H.L., "Dimensional Analysis and Theory of Models", John Wiley and Sons, New York, 1954.
- 2) Merrit, F. S., "Structural Steel Designers Handbook", McGraw-Hill, New York, 1972.
- 3) Bathe, K., Wilson, E.L., Peterson, F.E., "SAP IV: A Structural Analysis Program for Static and Dynamic Response of Linear Systems", National Technical Information Service, 1973.
- 4) Gaylord, E.H., and Gaylord C.N., "Structural Engineering Handbook", McGraw-Hill, New York, 1968.
- 5) Shukla, S.N. and Ojalvo, M., "Lateral Buckling of Parabolic Arches with Tilting Loads", Journal of the Structural Division, ASCE, June, 1971.
- 6) Tokarz, F.J., "Experimental Study of Lateral Buckling of Arches", Journal of the Structural Division, ASCE, February, 1971.
- 7) Godden, W.G., "The Lateral Buckling of Tied Arches", Institution of Civil Engineers, Proceedings, Vol. 4, paper No. 5965, August, 1954.

MICHIGAN STATE UNIV. LIBRARIES



31293000759179